

Room temperature *in-situ* preparation of hydrazine-linked covalent organic frameworks coated capillaries for separation and determination of polycyclic aromatic hydrocarbons

Yanli Zhang^{1,2}, Wenjuan Lv (✉)^{1,2}, Fangling Wang^{1,2}, Xiao Niu^{1,2}, Guoxiu Wang^{1,2}, Xuequan Wu^{1,2}, Xiaoyun Zhang (✉)^{1,2}, Xingguo Chen^{1,2}

1 State Key Laboratory of Applied Organic Chemistry, Lanzhou University, Lanzhou 730000, China

2 College of Chemistry and Chemical Engineering, Lanzhou University, Lanzhou 730000, China

© Higher Education Press 2023

Abstract Covalent organic frameworks (COFs) have been increasingly used in capillary electrochromatography due to their excellent characteristics. In this work, hydrazine-linked TFPB-DHzDS (TFPB: 1,3,5-tris(4-formylphenyl)benzene; DHzDS: 2,5-bis(3-(ethylthio)propoxy)terephthalohydrazide) was first synthesized by a simpler and easier method at room temperature and introduced into capillary electrochromatography as coating material. The TFPB-DHzDS coated capillaries were prepared by an *in-situ* growth process at room temperature. After optimizing the coating concentration and experimental conditions of capillary electrochromatography, baseline separation of two groups of polycyclic aromatic hydrocarbons was achieved based on the TFPB-DHzDS coated capillary. And the established method was used successfully to determine PAHs in natural water and soil samples. The spiked recoveries of polycyclic aromatic hydrocarbons in these samples ranged from 90.01% to 111.0%, indicating that the method is reliable and could detect polycyclic aromatic hydrocarbons in natural samples. Finally, molecular simulation was applied to study and visualize the interaction between the analytes and coating COF materials to investigate the molecular level separation mechanism further.

Keywords hydrazine-linked TFPB-DHzDS, *in-situ* growth method, open-tubular capillary electrochromatography, molecular simulations

1 Introduction

Covalent organic frameworks (COFs) are a new class of porous crystalline materials, covalently bonded by rigid and symmetric organic units. COFs have excellent characteristics of predictable structures, ordered channels, tunable porosity, large specific surface area, easy functionalization, environmental friendliness and good chemical and thermal stability. Since first reported in 2005 [1], the studies of COFs' building blocks, connection types and synthesis methods have made remarkable progress. Moreover, COFs have been used in an unprecedented expansion in applications, such as catalysis [2], gas storage [3], drug delivery [4] and sensing [5]. Recently, due to their unique properties, COFs materials have also been successfully applied in analytical chemistry such as solid phase extraction [6–8], separation [9–11] and spectroscopic detection [12].

So far, most COFs materials have been synthesized by solvothermal synthesis [13]. However, traditional solvothermal synthesis is tedious and toxic. Thus, it is very significant to develop a simple and environment-friendly COFs synthesis method. In 2019, Zhang et al. [14] proposed spherical imine-linked COFs with controllable size, which were synthesized at room temperature in acetonitrile using acetic acid as a catalyst. Furthermore, in 2020, Loh's group [15] found that the building units of hydrazide with longer side chains could form intra- and inter-layer hydrogen bonds when forming hydrazine-linked COFs, which would accelerate the crystallization of COFs. Therefore, we supposed that hydrazine-linked COFs with longer side

Received May 3, 2022; accepted September 3, 2022

E-mails: lvwenj@lzu.edu.cn (Lv W.), xyzhang@lzu.edu.cn (Zhang X.)

chains could also be synthesized conveniently at room temperature.

Capillary electrochromatography (CEC) features high separation efficiency, good selectivity, low sample consumption and fast analysis. It combines the advantages of capillary electrophoresis and high performance liquid chromatography. The preparation of the open-tubular column (OT) in CEC was divided into the post-modification [16] method and *in-situ* preparation [17]. Compared to the post-modification method, the *in-situ* preparation of COFs-coated capillaries is a simpler process under milder conditions. More importantly, the prepared COFs-coated capillaries are more uniform.

As a class of environmental endocrine disruptors, polycyclic aromatic hydrocarbons (PAHs) originate mainly from the incomplete combustion of coal, petroleum, coal tar, and tobacco [18–23]. Through wet and dry deposition, atmospheric PAHs and their derivatives can enter different environmental media such as soil, water, dust, and food [24,25]. Excessive exposure to such pollutants can cause severe damage to the human respiratory, circulatory and nervous systems, liver and kidneys [26,27], which necessitates their determination in the environment. However, since such PAHs are neutral substances, the commonly used CEC is unable to achieve their separation. Hence, it is necessary to achieve CEC separation of PAHs with the help of new coating materials. According to the particular molecular structure features of PAHs, 1,3,5-tris(4-formylphenyl)benzene (TFPB) was chosen as one of the coating COF materials' building blocks. This compound has a large π conjugated structure to strengthen the $\pi-\pi$ interaction between PAHs and the coating material, thus promoting the separation efficiency of CEC.

With the rapid development of computer science, molecular simulation has become one of the most important and active frontier research fields. It has played a significant role in studying the interaction between receptor and ligand, virtual drug screening and new drugs synthesis [28,29]. Here, molecular simulation was introduced to study and visualize the interaction between the analytes and coating COF materials to further investigate the molecular level separation mechanism.

Therefore, in this work, we attempted to develop a simpler method to synthesize the COF TFPB-DHzDS (DHzDS: 2,5-bis(3-(ethylthio)propoxy)terephthalohydrazide) at room temperature. A simple and fast *in-situ* method was built for preparing TFPB-DHzDS coated capillary at room temperature as well as an OT-CEC system to successfully analyze PAHs in natural samples. Furthermore, molecular simulation was used to investigate the separation mechanism at a molecular level.

2 Experimental

2.1 Preparation of TFPB-DHzDS and TFPB-DHzDS coated capillary with different thicknesses

The synthesis of TFPB followed the procedure in Fig. S1 (cf. Electronic Supplementary Material, ESM). The synthesis of TFPB-DHzDS (Fig. S2, cf. ESM) included the following steps: Firstly, DHZDS (26 mg, 0.06 mmol) and TFPB (16 mg, 0.10 mmol) were preloaded in a centrifuge tube. After adding 5 mL acetonitrile, the mixed solution was sonicated until it was clear. After that, 12 mol·L⁻¹ acetic acid was added to the above solution and shaken vigorously for 30 s. Finally, the tube was sealed and stored at room temperature for 72 h to get a white precipitate. Then, the precipitate was washed three times with anhydrous tetrahydrofuran and methanol, respectively. After drying at 60 °C for 8 h, the white product representing COF TFPB-DHzDS was collected.

The preparation process of the TFPB-DHzDS coated capillary is illustrated in Fig. 1. Firstly, the bare capillary was washed with methanol, ultrapure water and NaOH (1.0 mol·L⁻¹) for 10 min, 10 min and 15 min, respectively, and then heated at 100 °C for 2 h in an oven. After that, the capillary was rinsed with HCl (0.5 mol·L⁻¹) for 30 min, followed by rinsing with methanol, acetone and ultrapure water for 10 min each. After drying under nitrogen, the capillary was heated for 1 h at 150 °C. Secondly, the pretreated capillary was pumped fully with 5% (v/v) 3-glycidoxypropyltrimethoxysilane (GLYMO)-toluene solution and heated at 100 °C for 6 h to get a GLYMO-coated capillary. Then, it was washed with toluene, methanol and acetone for 10 min, respectively, and dried under nitrogen. Thirdly, three mixtures were prepared by adding DHZDS (8.7 mg, 0.02 mmol) and TFPB (5.3 mg, 0.014 mmol), DHZDS (4.3 mg, 0.01 mmol) and TFPB (2.7 mg, 0.007 mmol) and DHZDS (2.2 mg, 0.005 mmol) and TFPB (1.4 mg, 0.0035 mmol) into three 10 mL centrifuge tubes. Acetonitrile (1.65 mL) and acetic acid solution (0.1 mL, 12 mol·L⁻¹) were added to form 8, 4, 2 mg·mL⁻¹ TFPB-DHzDS stock solutions. Then, 1 and 0.5 mg·mL⁻¹ stock solutions were gradually diluted with 2 mg·mL⁻¹ stock solutions. After preparing the stock solutions, the GLYMO-coated capillary was immediately filled with the stock solutions and sealed on both ends. Then the anterior capillaries were placed on the experiment table for 72 h at room temperature. After rinsing the residual TFPB-DHzDS from the capillary with methanol and acetone (10 min), the TFPB-DHzDS coated capillaries were dried with nitrogen and protected under a nitrogen atmosphere until used.

2.2 Preparation of standard solutions

Stock solutions (1 mg·mL⁻¹) of PAHs and thiourea in

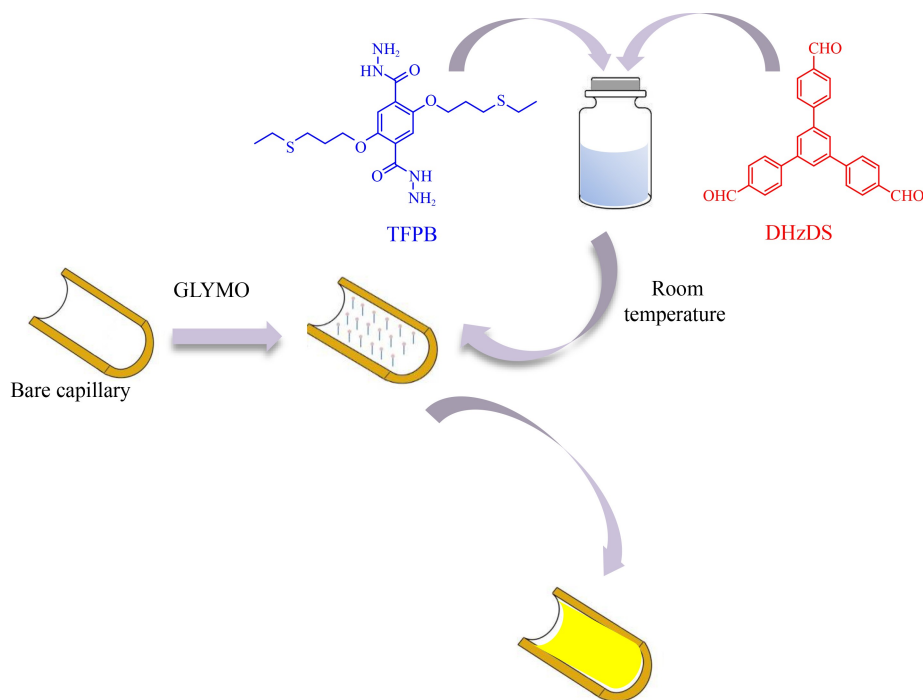


Fig. 1 Schematic diagram for the preparation of the TFPB-DHzDS coated capillary.

acetonitrile were kept at 4 °C in a refrigerator. Before being injected into the CEC system, all solutions had to be degassed under ultra-sonication (5 min).

2.3 Real samples preparation

Water samples were taken from the fountain at Lanzhou University and the Yellow River. After filtering with a 0.22 μm pore size nylon membrane, 1 mL of the sample solution was added into a centrifuge tube and dried under nitrogen. Then, it was re-dissolved using a 1 mL buffer solution.

Soil samples were taken from the banks of the Yellow River. Firstly, soil samples were air-dried and cleaned by moving plant residues and other inclusions inside. Then the samples were ground in an agate mortar to achieve good mixing and uniformity. Afterwards, 50 g of the soil sample was dispersed in 20 mL acetonitrile solvent and ultrasonicated for 30 min. Then the filtered solutions were dried by a rotary evaporator and the residues were dissolved in 5 mL buffer solution. All sample solutions were sealed and stored in brown bottles at 4 °C.

3 Results and discussion

3.1 Characterization of TFPB-DHzDS and TFPB-DHzDS coated capillary

Figure 2 indicates the characterization results of TFPB-DHzDS. The PXRD pattern is shown in **Fig. 2(a)**. The presence of 100, 110, and 200 crystal planes is consistent

with the COF TFPB-DHzDS synthesized by the solvothermal synthesis reported in the literature [30]. **Figure 2(b)** demonstrates that the material had peak absorption at 1602 cm⁻¹ for the C=N stretching vibration, proving that TFPB-DHzDS was successfully synthesized at room temperature. SEM images indicate that the morphology of TFPB-DHzDS synthesized under the same conditions is also reticulated (shown in **Figs. 2(c, d)**).

The N₂ adsorption and desorption isotherm profiles and pore size distribution of TFPB-DHzDS have been shown in Fig. S3 (cf. ESM). The BET specific surface area of TFPB-DHzDS is 236 m²·g⁻¹. Subsequently, SEM was used to observe the inner wall of the TFPB-DHzDS coated capillaries with different pass-through monomer concentrations. The results are illustrated in **Fig. 3**.

Figure 3 shows SEM images of the inner wall of the capillary before and after being coated. It is evident that the inner surface is very smooth before the coating. In comparison, after the coating, the TFPB-DHzDS COF is evenly distributed on the inner wall and the coating thickness increases as the pass-through monomer concentration increases. The morphology of TFPB-DHzDS synthesized in and out of the capillary is consistent, which fully proves that TFPB-DHzDS COF was successfully grown *in-situ* on the inner wall of the capillary at room temperature. **Figure S4** (cf. ESM) shows SEM images of the cross-sections of bare capillary and the TFPB-DHzDS coated capillaries with 0.5, 1.0, 2.0, 4.0 and 8.0 mg·mL⁻¹ monomer concentrations. It can also be seen that there is a corresponding increase in coating thickness with increasing coating concentration, which is good proof that the TFPB-DHzDS coated capillaries were

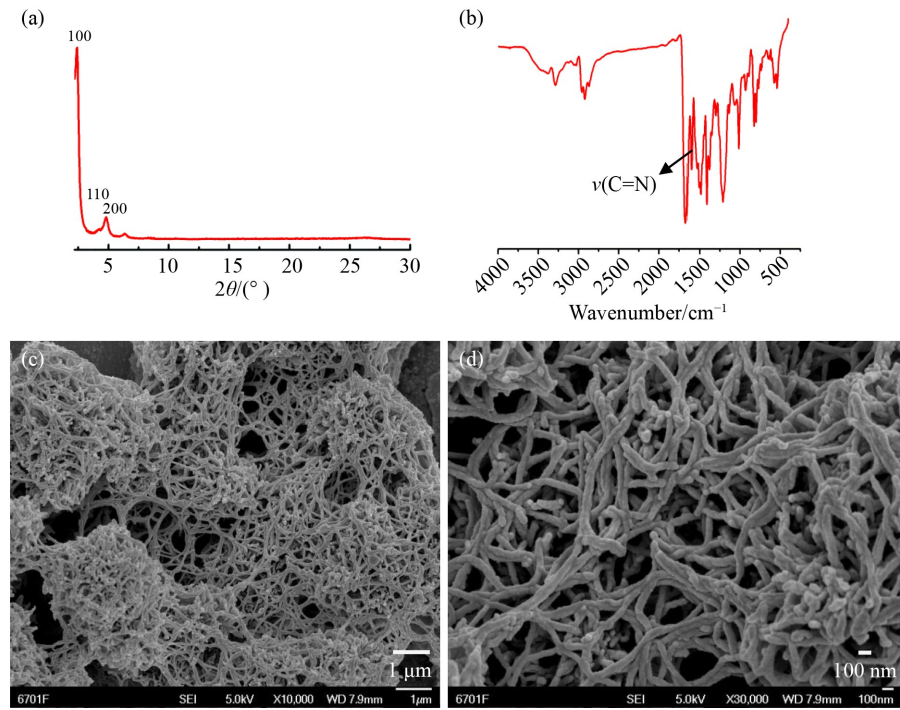


Fig. 2 (a) PXRD, (b) FT-IR, and (c, d) SEM images of COF TFPB-DHzDS synthesized at room temperature; (c) at 10000 magnification and (d) at 30000 magnification.

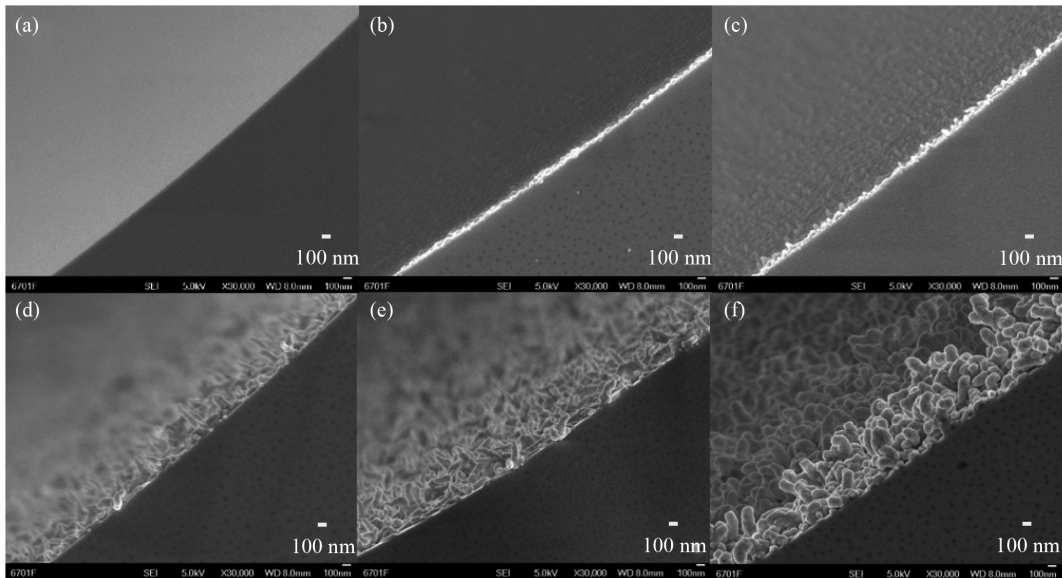


Fig. 3 SEM images of the inner walls of TFPB-DHzDS coated capillaries prepared at different pass-through monomer concentrations: (a) bare capillary; (b) 0.5 $\text{mg}\cdot\text{mL}^{-1}$; (c) 1.0 $\text{mg}\cdot\text{mL}^{-1}$; (d) 2.0 $\text{mg}\cdot\text{mL}^{-1}$; (e) 4.0 $\text{mg}\cdot\text{mL}^{-1}$; (f) 8.0 $\text{mg}\cdot\text{mL}^{-1}$.

successfully prepared by the proposed *in-situ* growth method at room temperature.

3.2 Effect of electroosmotic flow (EOF) on separation

The concentration and pH of buffer solution, organic additive content, and operating voltage affect the variation of EOF, the main driving force of CEC, and then further affect the separation of CEC. Hence, we

examined the influences of these factors on EOF. As shown in Fig. S5 (cf. ESM), the EOF of the coated capillary decreased, indicating that the COFs material had successfully grown on the capillary and covered the Si-OH of the bare capillary, thus leading to a decrease of charge density on the inner capillary wall and then a reduction in EOF. In addition, the EOF of the capillaries, both before and after coating, increases with the pH of buffer solution and operating voltage rising and decreases

with the concentration of buffer solution and organic additive content rising.

3.3 CEC separation

Using the first group of PAHs as a model, the separation ability of the coated capillary prepared at different monomer concentrations on the same analytes was evaluated. As illustrated in Fig. 4, the separation ability became lower when the monomer concentration was less than $2.0 \text{ mg}\cdot\text{mL}^{-1}$ and the baseline separation of analytes was not achieved with a smaller coating thickness. This result proved that the interaction force between the COF coating and analytes became weaker with the decrease of the monomer concentration and the coating thickness. While the monomer concentration was greater than $2.0 \text{ mg}\cdot\text{mL}^{-1}$, the adsorption of the analytes by the coating became stronger and stronger and the spectral peak was seriously trailing, which resulted in a longer migration time. Therefore, after overall consideration, the TFPB-DHzDS coated capillary with $2.0 \text{ mg}\cdot\text{mL}^{-1}$ monomer concentration was regarded as the optimal coating capillary to finish subsequent CEC experiments.

Subsequently, we optimized the separation conditions for these two groups of PAHs. Considering that the coating material was hydrazine-linked COFs, which were stable under both acid and alkaline conditions, we chose borax as the running buffer solution. The running buffer concentration can influence Joule heat and ionic strength of the separation system, thereby affecting the peak shape and separation efficiency. Therefore, we first optimized the concentration of borax. As shown in Fig. S6 (cf. ESM), when borax concentration was $10 \text{ mmol}\cdot\text{L}^{-1}$, the two PAH groups achieved baseline separation. Hence, $10 \text{ mmol}\cdot\text{L}^{-1}$ was chosen as the optimum borax buffer concentration.

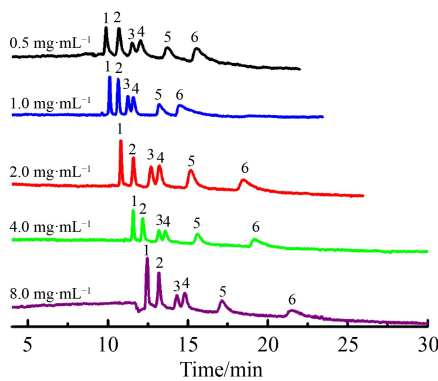


Fig. 4 Effect of TFPB-DHzDS COFs coated capillaries with different monomer concentration for separation of PAHs. Operating conditions: $10 \text{ mmol}\cdot\text{L}^{-1}$ borax, 32.5% acetonitrile, $\text{pH} = 10.00$ ($0.5\text{--}4.0 \text{ mg}\cdot\text{mL}^{-1}$); $10 \text{ mmol}\cdot\text{L}^{-1}$ borax, 37.5% acetonitrile, $\text{pH} = 10.00$ ($8.0 \text{ mg}\cdot\text{mL}^{-1}$). Spectral peak designation: 1. NAP; 2. ANA; 3. ANT; 4. PHE; 5. PYR; 6. BPH. Operating voltage: $+20 \text{ kV}$; detection wavelength: 226 nm .

Buffer pH value can impact the dissociation extent of Si-OH on the inner wall of the capillary, affecting the EOF and separation efficiency of analytes. Therefore, we also optimized the buffer pH value (shown in Fig. S7, cf. ESM). The EOF increased with the buffer pH value rising, resulting in a shorter retention time of analytes and vice versa. The baseline separation was achieved for the first group of PAHs when $\text{pH} = 10.00$. Moreover, PYR and BPH showed noticeable trailing when the pH was less than 10.00 , and the peak shape became poor when the pH was greater than 10.00 . Therefore, we chose 10.00 as the optimum pH of the buffer solution. For the second group of PAHs, the baseline separation was achieved at $\text{pH } 9.50\text{--}11.00$. Considering the analytes' peak shape and retention time, we chose 10.50 as the optimal pH for the second group of analytes.

The operating voltage also affects the EOF of the separation system. The smaller voltage caused the spectral peak trailing and caused the EOF to decrease, which resulted in the migration time increase. In contrast, too large voltage made the EOF increase and the baseline separation of analytes could not be achieved. So, the running voltage was also optimized in the separation system, as shown in Fig. S8 (cf. ESM). We selected $+20 \text{ kV}$ as the optimal separation voltage of two groups analytes for subsequent experiments.

The organic additives can not only improve the peak shape of analytes but also promote the CEC separation. PAHs had a strong adsorption capacity with the coating material on the capillary inner wall due to their greater hydrophobicity ($\log K_{ow}$). Based on this, we selected acetonitrile with a strong elution capacity as an organic additive to enhance the elution capacity of the buffer solution. As shown in Fig. S9 (cf. ESM), the elution capacity increases with the increase of acetonitrile content. For these two groups of analytes, baseline separation could not be achieved at 37.5% and 50.0% acetonitrile content. The acetonitrile concentrations of 27.5% and 40.0% caused the poor peak shape of analytes and the longer migration time. However, two groups of analytes achieved the baseline separation at 32.5% and 45.0% acetonitrile content. the 32.5% and 45.0% acetonitrile concentrations were selected as the optimal amount of organic additive for CEC separation.

As shown in Figs. 5(a) and 5(b), two groups of analytes achieved the baseline separation under their respective optimal conditions on the TFPB-DHzDS-coated capillary. The chromatographic data of the two PAH groups under optimum separation conditions are shown in Table S1 (cf. ESM). Their elution order is relative to their $\log K_{ow}$. The analyte with a bigger $\log K_{ow}$ has a longer migration time (Table S2, cf. ESM), except for PHE and ANT. The likely reason is that ANT has greater molecular size and volume than PHE, which would impede to some extent the passing through the holes of the coating material and

result in longer migration time although both PHE and ALT have the same $\log K_{ow}$.

3.4 Separation performance of the TFPB-DHzDS coated capillary

The separation performance of the TFPB-DHzDS coated capillary was further compared with the bare capillary. As exhibited in Figs. 5(a, b), two PAH groups were baseline separated within 20 min based on the TFPB-DHzDS coated capillary. At the same time, all analytes did not show satisfactory separation performances based on the bare capillary and GLYMO-coated capillary (Figs. 5(c, d)), indicating that the coating material provided good separation capability for the CEC separation. Subsequently, we established the standard curves of these

PAHs under optimal separation conditions. These PAHs showed good linear correlation between their concentrations and peak areas in the linear range. The relative parameters are listed in Table 1. The results showed correlation coefficients $R^2 \geq 0.9824$, limits of detection (LODs) ranging from 0.04 to $0.39 \mu\text{g}\cdot\text{mL}^{-1}$ and limits of quantification (LOQs) ranging from 0.14 to $1.31 \mu\text{g}\cdot\text{mL}^{-1}$.

3.5 Repeatability and stability of the TFPB-DHzDS coated capillary

To examine the repeatability of the coated capillary, the intra-day ($n = 3$), inter-day ($n = 3$) and column-to-column ($n = 3$) reproducibility of two PAH groups were evaluated and the data are presented in Table S3 (cf. ESM). The

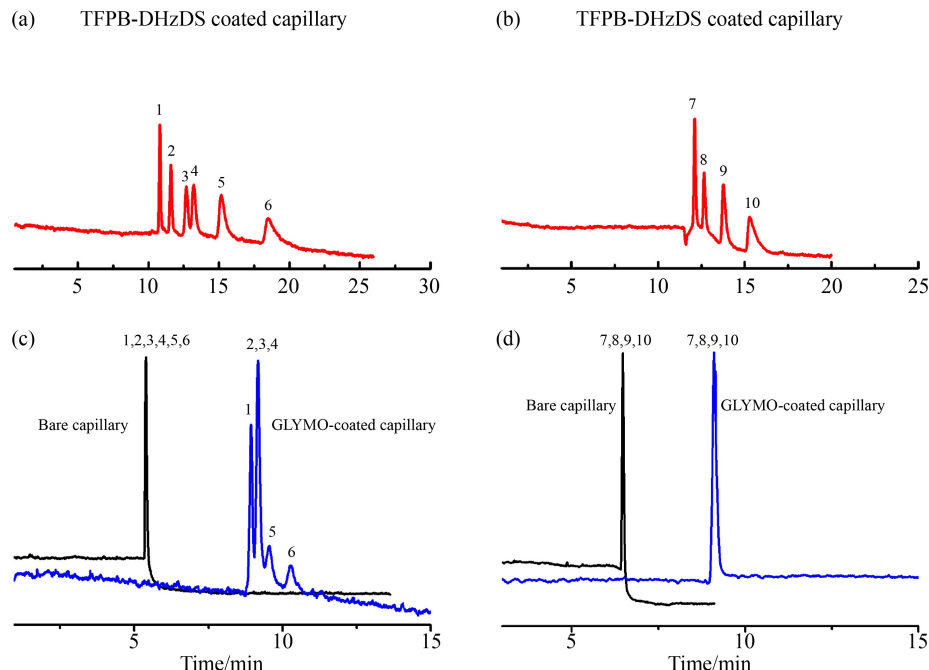


Fig. 5 (a, b) Comparison of the separation of the two groups PAHs based on the TFPB-DHzDS coated capillary; (c, d) based on the bare capillary and GLYMO-coated capillary. Conditions: $10 \text{ mmol}\cdot\text{L}^{-1}$ borax with 27.5% acetonitrile, pH = 10.00 for (a) and (c); $10 \text{ mmol}\cdot\text{L}^{-1}$ borax with 45.0% acetonitrile, pH = 10.50 for (b) and (d). Running voltage was +20 kV.

Table 1 Linear range, linear equation, correlation coefficient, LOD and LOQ of PAHs

Analyte	Linearity/(\mu\text{g}\cdot\text{mL}^{-1})	Linear equation ^{a)}	R^2	LOD ^{b)} (\mu\text{g}\cdot\text{mL}^{-1})	LOQ ^{c)} (\mu\text{g}\cdot\text{mL}^{-1})
NAP	0.20–100.00	$Y = 6065.46X + 99.25$	0.9924	0.06	0.19
ANA	0.20–100.00	$Y = 7905.02X - 569.37$	0.9997	0.04	0.15
ANT	1.00–100.00	$Y = 1458.97X - 1978.34$	0.9899	0.24	0.79
PHE	1.00–100.00	$Y = 1059.92X - 551.51$	0.9866	0.33	1.09
PYR	1.00–100.00	$Y = 1812.32X - 252.53$	0.9981	0.19	0.64
BPH	2.50–100.00	$Y = 886.41X - 820.70$	0.9835	0.39	1.31
FLU	0.50–100.00	$Y = 1897.61X - 928.69$	0.9952	0.16	0.52
FLT	0.25–100.00	$Y = 4742.37X - 317.77$	0.9824	0.06	0.21
BaA	0.25–100.00	$Y = 6340.83X - 965.01$	0.9999	0.05	0.16
BbF	0.25–100.00	$Y = 6818.69X + 2713.46$	0.9937	0.04	0.14

a) Y : peak area; X : concentration of analyte; b) calculated on the basis of $3s/k$ (s was the deviation of baseline; k was the slope of the linear equation); c) calculated on the basis of $10s/k$.

RSDs of retention time ranged from 0.50% to 2.79%, 1.12% to 4.41% and 2.12% to 5.29% for intra-day, inter-day and column-to-column, respectively. The RSDs of peak area for PAHs have a range of 0.07%–4.13%, 1.38%–4.87% and 3.07%–9.47% for intra-day, inter-day and column-to-column, respectively. The results demonstrate that the TFPB-DHzDS coated capillary has good repeatability.

As shown in Fig. 6, PAHs achieved baseline separation after 200 runs on the TFPB-DHzDS coated capillary and the peak time and peak shape did not change significantly, proving that the TFPB-DHzDS coated capillary has a long service life and good stability.

3.6 Real samples analysis

We collected three real samples from the Yellow River water and soil and the fountain water on the Lanzhou University campus to detect PAHs in these samples. The results showed that PAHs were not detected in the three samples. The reason may be related to PAHs concentrations below the above LODs. We also conducted spiked recovery experiments on these three samples. As shown in Tables S4–S6 (cf. ESM), the spiked recoveries of PAHs in these three real samples at low, medium and high concentrations were 90.11%–109.9%, 90.01%–109.6% and 91.43%–111.0%, respectively. The results also indicated that the method could be used to detect PAHs in natural samples.

3.7 Possible separation mechanism

Based on the experimental results of CEC separation, the molecular simulation was used further to investigate the separation mechanism at a molecular level. All simulations were preceded by Autodock 4.2 and the favorite binding positions of the PAHs interacting with COFs were obtained. As shown in Fig. 7, both groups of PAHs could pass through the porous channels of TFPB-DHzDS and interact with COFs. All the PAHs have an

edge-to-face configuration when they have π – π interactions with COFs. The binding energies between PAHs and COF TFPB-DHzDS were also calculated and are presented in Figs. 7(a) and 7(b). It is demonstrated that PAHs which bind to TFPB-DHzDS with lower binding energy migrated with a shorter migration time and vice versa. PYR and BPH were exceptions. Although BPH interacts with COF by lower binding energy, it still was eluted later. This result may be due to the BPH's bigger molecular size and molecular volume, which make it more difficult for BPH to get through the porous channels of TFPB-DHzDS. The $\log K_{ow}$, molecular size and molecular volume of PAHs are shown in Table S2. As discussed at the end of Section 3.3 CEC separation, the $\log K_{ow}$, that is, the hydrophobicity, also greatly influenced the separation of PAHs. Thus, the separation mechanism of CEC for two groups of PAHs based on the TFPB-DHzDS coating may be a synergistic effect of π – π interactions, hydrophobic interactions between PAHs and the coating material and size selectivity of the coating material.

4 Conclusions

In this work, a new method was successfully developed for *in-situ* growth of hydrazine-linked COF TFPB-DHzDS on the inner wall of capillary and the preparation of TFPB-DHzDS uniformly coated capillaries at room temperature. Two groups of PAHs were baseline separated on this coated capillary with high separation efficiency. Moreover, good stability and reproducibility of the coated capillary were demonstrated. A new method was built for analyzing PAHs in natural water and soil samples. The separation mechanism was investigated in detail and visualized at a molecular level by molecular simulation. This work expands the application of hydrazine-linked COFs in chromatographic separations and provides a simple method for preparing the COFs coated capillaries at room temperature.

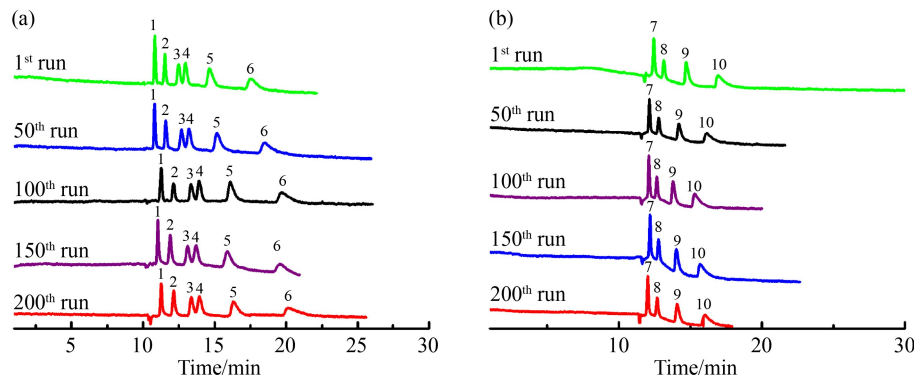


Fig. 6 Electrophoretic spectra of two groups of PAHs based on TFPB-DHzDS coated capillary for 200 runs. Conditions: (a) $10 \text{ mmol}\cdot\text{L}^{-1}$ borax with 32.5% acetonitrile, $\text{pH} = 10.00$; (b) $10 \text{ mmol}\cdot\text{L}^{-1}$ borax with 45.0% acetonitrile, $\text{pH} = 10.50$. Running voltage: +20 kV; detection wavelength: 226 nm.

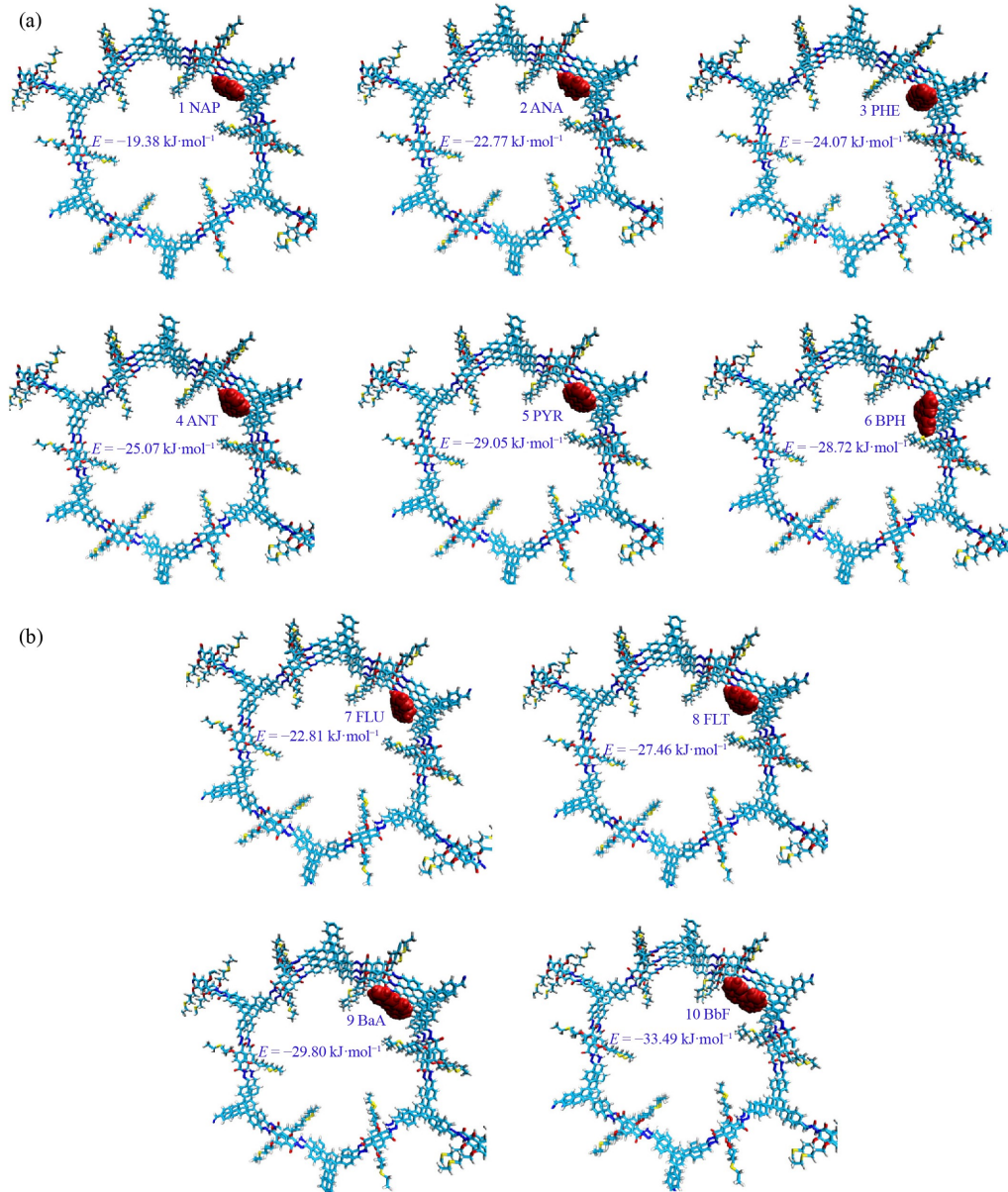


Fig. 7 Molecular simulations of the interactions of ten PAHs with COF TFPB-DHzDS coated capillary column: (a) 1 NAP, 2 ANA, 3 PHE, 4 ANT, 5 PYR, 6 BPH; (b) 7 FLU, 8 FLT, 9 BaA, 10 BbF. Carbon atoms of COF TFPB-DHzDS were in cyan, nitrogen atoms in blue, oxygen atoms in red and hydrogen atoms in white; all PAHs molecules are shown in red; the binding energies between PAHs and COF TFPB-DHzDS are shown in blue.

Acknowledgements The authors thank the National Natural Science Foundation of China (Grant Nos. 21705064 and 21675068) for financial support.

Electronic Supplementary Material Supplementary material is available in the online version of this article at <https://dx.doi.org/10.1007/s11705-022-2252-1> and is accessible for authorized users.

References

- Cote A P, Benin A I, Ockwig N W, O'Keeffe M, Matzger A J, Yaghi O M. Porous, crystalline, covalent organic frameworks. *Science*, 2005, 310(5751): 1166–1170
- Li Y, Pei B, Chen J J, Bing S S, Hou L X, Sun Q, Xu G, Yao Z K, Zhang L. Hollow nanosphere construction of covalent organic frameworks for catalysis: (Pd/C)@TpPa COFs in Suzuki coupling reaction. *Journal of Colloid and Interface Science*, 2021, 591: 273–280
- Liu X M, Lim G J H, Wang Y X, Zhang L, Mullangi D, Wu Y, Zhao D, Ding J, Cheetham A K, Wang J. Binder-free 3D printing of covalent organic framework (COF) monoliths for CO₂ adsorption. *Chemical Engineering Journal*, 2021, 403(1): 126333
- Zhao K, Gong P W, Huang J, Huang Y, Wang D D, Peng J Y, Shen D Y, Zheng X F, You J M, Liu Z. Fluorescence turn-off magnetic COF composite as a novel nanocarrier for drug loading and targeted delivery. *Microporous and Mesoporous Materials*,

- 2021, 311: 110713
- 5. Guan Q, Guo H, Xue R, Wang M, Wu N, Cao Y, Zhao X, Yang W. Electrochemical sensing platform based on covalent organic framework materials and gold nanoparticles for high sensitivity determination of theophylline and caffeine. *Mikrochimica Acta*, 2021, 188(3): 85
 - 6. Wu M, Chen G, Liu P, Zhou W, Jia Q. Polydopamine-based immobilization of a hydrazone covalent organic framework for headspace solid-phase microextraction of pyrethroids in vegetables and fruits. *Journal of Chromatography A*, 2016, 1456: 34–41
 - 7. Wang H, Jiao F, Gao F, Lv Y, Wu Q, Zhao Y, Shen Y, Zhang Y, Qian X. Titanium(IV) ion-modified covalent organic frameworks for specific enrichment of phosphopeptides. *Talanta*, 2017, 166: 133–140
 - 8. Chen Y, Chen Z. COF-1-modified magnetic nanoparticles for highly selective and efficient solid-phase microextraction of paclitaxel. *Talanta*, 2017, 165: 188–193
 - 9. Feng L L, Qian C, Zhao Y L. Recent advances in covalent organic framework-based nanosystems for bioimaging and therapeutic applications. *ACS Materials Letters*, 2020, 2(9): 1074–1092
 - 10. Zhou L, Lun J, Liu Y, Jiang Z, Di X, Guo X. *In-situ* immobilization of sulfated- β -cyclodextrin as stationary phase for capillary electrochromatography enantioseparation. *Talanta*, 2019, 200: 1–8
 - 11. Sun W Q, Liu Y K, Zhou W, Li Z T, Chen Z L. *In-situ* growth of a spherical vinyl-functionalized covalent organic framework as stationary phase for capillary electrochromatography-mass spectrometry analysis. *Talanta*, 2021, 230: 122330
 - 12. Yu Y X, Li G L, Liu J H, Yuan D Q. A recyclable fluorescent covalent organic framework for exclusive detection and removal of mercury(II). *Chemical Engineering Journal*, 2020, 401: 126139
 - 13. Geng K, He T, Liu R, Dalapati S, Tan K T, Li Z, Tao S, Gong Y, Jiang Q, Jiang D. Covalent organic frameworks: design, synthesis, and functions. *Chemical Reviews*, 2020, 120(16): 8814–8933
 - 14. Ma W D, Zheng Q, He Y T, Li G R, Guo W J, Lin Z, Zhang L. Size-controllable synthesis of uniform spherical covalent organic frameworks at room temperature for highly efficient and selective enrichment of hydrophobic peptides. *Journal of the American Chemical Society*, 2019, 141(45): 18271–18277
 - 15. Li X, Qiao J, Chee S W, Xu H S, Zhao X, Choi H S, Yu W, Quek S Y, Mirsaidov U, Loh K P. Rapid, scalable construction of highly crystalline acylhydrazone two-dimensional covalent organic frameworks via dipole-induced antiparallel stacking. *Journal of the American Chemical Society*, 2020, 142(10): 4932–4943
 - 16. Zhao L, Lv W, Niu X, Pan C, Chen H, Chen X. An azine-linked covalent organic framework as stationary phase for separation of environmental endocrine disruptors by open-tubular capillary electrochromatography. *Journal of Chromatography A*, 2020, 1615: 460722
 - 17. Bao T, Wang S, Zhang N, Zhang J. Facile synthesis and immobilization of functionalized covalent organic framework-1 for electrochromatographic separation. *Journal of Chromatography A*, 2021, 1645: 462130
 - 18. Hu Y, Chen B, Qian J, Jin L, Jin T, Lu D. Occupational coke oven emissions exposure and risk of abnormal liver function: modifications of body mass index and hepatitis virus infection. *Occupational and Environmental Medicine*, 2010, 67(3): 159–165
 - 19. Auer R, Concha-Lozano N, Jacot-Sadowski I, Cornuz J, Berthet A. Heat-not-burn tobacco cigarettes: smoke by any other name. *JAMA Internal Medicine*, 2017, 177(7): 1050–1052
 - 20. Kim D Y, Lee B E, Shin H S. Determination of polycyclic aromatic hydrocarbons (PAHs) in smoking cessation aids by using high-performance liquid chromatography. *Analytical Biochemistry*, 2021, 617(15): 114119
 - 21. Wang X, Wang C, Gong P, Wang X, Zhu H, Gao S. Century-long record of polycyclic aromatic hydrocarbons from tree rings in the southeastern Tibetan Plateau. *Journal of Hazardous Materials*, 2021, 412: 125152
 - 22. Cieslik E, Fabianska M J. Preservation of geochemical markers during co-combustion of hard coal and various domestic waste materials. *Science of the Total Environment*, 2021, 768: 144638
 - 23. Schmutz A, Tremblay R, Audet C, Gagne J P, Pelletier E, St-Louis R. Under ice spills of conventional crude oil and diluted bitumen: physiological resilience of the blue mussel and transgenerational effects. *Science of the Total Environment*, 2021, 779: 146316
 - 24. Zhang M, Tang Z, Yin H, Meng T. Concentrations, distribution and risk of polycyclic aromatic hydrocarbons in sediments from seven major river basins in China over the past 20 years. *Journal of Environmental Management*, 2021, 280: 111717
 - 25. Tevlin A, Galarneau E, Zhang T, Hung H. Polycyclic aromatic compounds (PACs) in the Canadian environment: ambient air and deposition. *Environmental Pollution*, 2021, 271: 116232
 - 26. Sosnowski T R, Kolinski M, Gradon L. Interactions of benzo[a]pyrene and diesel exhaust particulate matter with the lung surfactant system. *Annals of Occupational Hygiene*, 2011, 55(3): 329–338
 - 27. Karami S, Boffetta P, Brennan P, Stewart P A, Zaridze D, Matveev V, Janout V, Kollarova H, Bencko V, Navratilova M, Szeszenia-Dabrowska N, Mates D, Gromiec J P, Sobotka R, Chow W H, Rothman N, Moore L E. Renal cancer risk and occupational exposure to polycyclic aromatic hydrocarbons and plastics. *Journal of Occupational and Environmental Medicine*, 2011, 53(2): 218–223
 - 28. Xu L, Zhou S, Yu K, Gao B, Jiang H, Zhen X, Fu W. Molecular modeling of the 3D structure of 5-HT(1A)R: discovery of novel 5-HT(1A)R agonists via dynamic pharmacophore-based virtual screening. *Journal of Chemical Information and Modeling*, 2013, 53(12): 3202–3321
 - 29. Yan W, Ling L, Wu Y, Yang K, Liu R, Zhang J, Zhao S, Zhong G, Zhao S, Jiang H, Xie C, Cheng J. Structure-based design of dual-acting compounds targeting adenosine A_{2A} receptor and histone deacetylase as novel tumor immunotherapeutic agents. *Journal of Medicinal Chemistry*, 2021, 64(22): 16573–16597
 - 30. Li X, Gao Q, Wang J, Chen Y, Chen Z H, Xu H S, Tang W, Leng K, Ning G H, Wu J, Xu Q H, Quek S Y, Lu Y, Loh K P. Tuneable near white-emissive two-dimensional covalent organic frameworks. *Nature Communications*, 2018, 9(1): 2335